Biophysical Journal, Volume *113*

Supplemental Information

A Cardiomyopathy Mutation in the Myosin Essential Light Chain Alters Actomyosin Structure

Piyali Guhathakurta, Ewa Prochniewicz, Osha Roopnarine, John A. Rohde, and David D. Thomas

A Cardiomyopathy Mutation in the Myosin Essential Light Chain Alters Actomyosin Structure

Piyali Guhathakurta, Ewa Prochniewicz, Osha Roopnarine, John A. Rohde and David D. Thomas*

Department of Biochemistry, Molecular Biology and Biophysics, University of Minnesota, Minneapolis, MN 55455

SUPPORTING MATERIAL

TR-FRET data analysis. Fluorescence waveforms were analyzed using non-linear least-squares fitting as described previously

(1,2). The observed donor-only waveform $F_{\mathrm{Dobs}}(t)$ was fitted by a simulation $F_{\mathrm{Dsim}}(t)$, consisting of a multiexponential decay $F_{\mathrm{D}}(t)$ (Fig 2, black) convolved with the instrument response function IRF(t) .

$$F_{\mathrm{D}}(\mathrm{t}) = \sum_{i=1}^{n} A_{\mathrm{i}} \exp(-t/\tau_{\mathrm{Di}}) ,$$

$$F_{\mathrm{Dsim}}(t) \int_{-\infty}^{+\infty} IRF(t-t')\, F_{\mathrm{D}}(t')\, dt', \qquad \textbf{Eq. S1}$$

where τ_{Di} are the donor-only fluorescence lifetimes (Fig. S1). The ensemble-average lifetime is given by

$$\langle \tau_{\mathrm{D}} \rangle = \sum_{i=1}^{n} A_{\mathrm{i}}\, \tau_{\mathrm{Di}} \,/\, \sum_{i=1}^{n} A_{\mathrm{i}} \qquad \textbf{Eq. S2}$$

The observed donor + acceptor waveform $F_{\mathrm{D+Aobs}}(t)$ was fitted by a multiexponential function using the same approach. The model-independent ensemble-average FRET efficiency $\langle E \rangle$, which is equivalent to the result of a steady-state fluorescence measurement (3), is given by

$$\langle E \rangle = 1 - \langle \tau_{\mathrm{D+A}} \rangle \,/\, \langle \tau_{\mathrm{D}} \rangle \, . \qquad \textbf{Eq. S3}$$

To resolve structural states, a distribution of donor-acceptor distances $\rho(r)$ was assumed:

$$F_{\mathrm{DA}}(t) = \int_{-\infty}^{+\infty} \rho(R) \cdot \sum_{i=1}^{n} A_{\mathrm{i}} \exp\{(-t/\tau_{\mathrm{Di}})(1+[R_{0\mathrm{i}}/R]^6)\}\mathrm{d}R, \qquad \textbf{Eq. S4}$$

where $R_{0\mathrm{i}}$ is the lifetime-weighted Förster distance.

$$R_{0\mathrm{i}}{}^6 = 9780^6 \mathrm{J} \kappa^2 n^{-4} k_{\mathrm{rad}} \tau_{\mathrm{Di}} \qquad \textbf{Eq. S5}$$

where J is the overlap integral between the donor emission and acceptor absorption spectra, n is the refractive index (1.4), κ^2 is the orientation factor (2/3, assuming random orientation), and k_{rad} is the radiative decay rate for the donor. Eq. S5 follows directly from the Förster theory's assumption (1) that the energy transfer rate constant k_{T} (= $R_{0\mathrm{i}}{}^6 R^{-6} / \tau_{\mathrm{Di}}$) depends on the donor-acceptor distance R but not on the donor-only lifetime τ_{Di}. R_0 between IAEDANS actin and

Dabcyl S1 was calculated as 3.3 nm, with a quantum yield 0.32 for IAEDANS actin (using quinine sulfate as the standard).

The distance distribution $\rho(R)$ (Eq. S4) was assumed to be a sum of n Gaussian components, each corresponding to a structural state of the actomyosin complex, with its central distances R_j, and a full width at half maximum Γ_j and mole fraction $\boldsymbol{x}_j$:

$$\rho(R) = \sum_{j=1}^{n} \boldsymbol{x}_j \sigma_j^{-1}(2\pi)^{-1/2} \exp(-[(R-R_j)/(2\sigma_j)]^2 \ , \ \sigma_j = \Gamma_j/[2*(2 \ln 2)^{1/2}], \qquad \textbf{Eq. S6}$$

$$\sum_{j=1}^{n} \boldsymbol{x}_j = 1.$$

The observed waveform $F_{D+Aobs}(t)$ was fitted by $F_{D+Asim}(t)$:

$$F_{D+A}(t) = (1 - X_B)F_D(t) + X_B F_{DA}(t),$$

$$F_{D+Asim}(t) = \int_{-\infty}^{+\infty} IRF(t - t') \cdot F_{D+A}(t')dt', \qquad \textbf{Eq. S7}$$

where X_B is the fraction of donor-labeled actin bound to and transferring energy to acceptor-labeled myosin. Thus binding (X_B) is determined independently of the mole fractions of resolved structural states (x_j in Eq. S6).

Donor-only fluorescence decays are best fit with 3 exponential components. The donor-only fluorescence decay $F_D(t)$ for IAEDANS actin (Fig.3), was fitted by a multiexponential function, with the result that three lifetime components are necessary and sufficient to fit the data (Eq. S1, n = 3), based on the residual plots (Fig. S1*A*) and the χ^2 values (sum of residuals at each data point Fig. S1*B*). The results show clearly that the fit is improved by increasing n from 2 to 3, but not by increasing n from 3 to 4. FRET efficiency (E) was calculated from average lifetime in model-independent analysis (Fig. 4), and the calculated interprobe distance from E was in good agreement with the R value obtained from model-dependent analysis described below and in methods. To increase precision in the FRET analysis, the three donor lifetime values were globally linked in model-dependent fitting.

Strongly bound complex shows best fit with a single attached state. To resolve structural states of the actomyosin complex in the absence of ATP, we used $F_D(t)$ as input, to fit $F_{D+Aobs}(t)$ and thus determine the mole-fraction of unbound donor ($1-X_B$) and interprobe distance distribution corresponding to the bound complex, $F_{DA}(t)$ (Eq. S4-Eq. S7). The goodness of fit

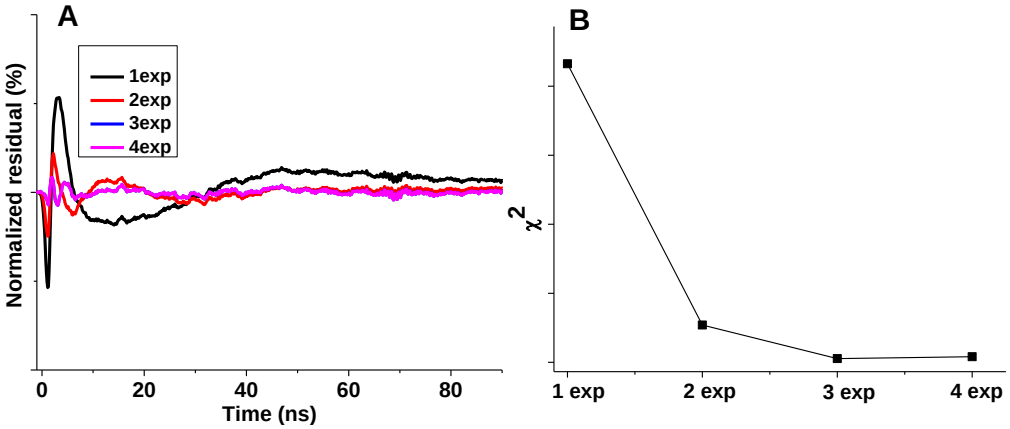

Fig. S1. Fluorescence lifetime fit of IAEDANS actin. (*A*). Normalized residual plot of fits with increasing n in (*B*). χ^2 values of lifetime components, showing that n = 3 is necessary and sufficient for the best fit to Eq. S1.

was evaluated to minimize χ^2, and the best fit to $F_{DA}(t)$ for the bound complex was obtained with a one-Gaussian component. A second Gaussian component did not improve the fit. Thus, in the rigor (no ATP) state, actomyosin is best described by a two-state model: a mole fraction ($1\text{-}X_B$) of unbound donor and a mole fraction X_S of the *S* state with a mean distance R_s and a FWHM of Γ_S. The distance (R_S) and width (Γ_S) were independent of the added myosin concentration (1-10 μM) to 2 μM actin (**Fig. S2**). In subsaturating conditions, the value of the mole fraction X_S obtained from the fitting was indistinguishable from the added myosin concentration; i.e., $X_B = X$s. In the presence of excess myosin, X_B was indistinguishable from 1.

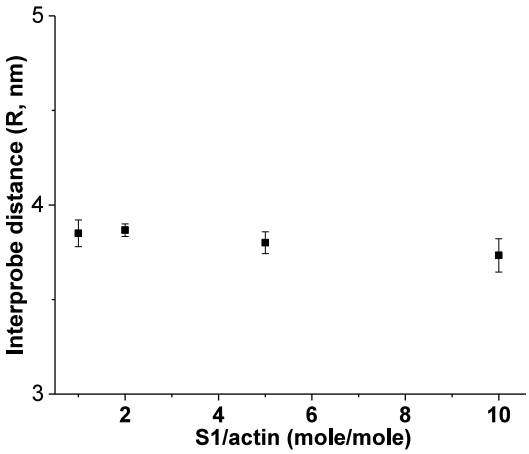

Fig. S2. Interprobe distance is independent of myosin concentrations in ***S*** complexes

Three states are necessary and sufficient to fit the steady-state TR-FRET data. To resolve structural states of the actomyosin complex in the presence of ATP, we also used $F_D(t)$ as input, to fit $F_{D+Aobs}(t)$ and determine the mole-fraction of unbound donor ($1\text{-}X_B$) and the interprobe distance distribution corresponding to $F_{DA}(t)$ (Eq. S4-Eq. S7). We tested models for $F_{DA}(t)$ with one, two, and three Gaussian components (Eq. S6 n = 1, 2, and 3). The goodness of fit was evaluated to minimize χ^2. The fit was consistently improved by increasing the number of components n in from 1 to 2, but not from 2 to 3 as described in our previous study (4). Thus two-Gaussian distance distributions were required to fit the TR-FRET data. We assumed that during the steady state of ATP hydrolysis the actomyosin complex is a mix of pre (*W*) and post power stroke (*S*) structural states represented by Gaussian distance distributions ρ_W and ρ_S with mole fractions X_W and X_S (Fig 5). Thus the actin-bound distance distribution is

$$\rho(R) = (X_W/X_B)\rho_W(R) + (X_S/X_B)\rho_S(R). \qquad \textbf{Eq. S8}$$

Thus in the presence of ATP, actomyosin is best described by a 3-state model: a mole fraction ($1\text{-}X_B$) of unbound donor, with the bound state (mole fraction X_B) described by a two-Gaussian distance distribution described by mole fraction X_S of the bound *S* state with a mean distance R_s and a FWHM of Γ_s, and a mole fraction X_W (= X_B - X_S) of the bound *W* state, with a mean distance R_W and a FWHM of Γ_W (Fig 5, red). The results are summarized in Fig 5. No improvement in the fit (decrease in χ^2) was obtained by allowing the *S* state parameters (R_S, Γ_S) to vary from the values observed in the absence of ATP (Fig. S6), so these parameters were fixed to those values in the analysis shown in Fig 5. The same two-Gaussian analysis was successfully applied previously to analyze FRET within smooth muscle myosin regulatory light chain (1) and the myosin relay helix (5), generating high-resolution structural information that was confirmed by independent molecular dynamics simulations (1) or by dipolar electron–electron resonance (DEER) EPR spectroscopy(5).

Mass Spectrometry. Mass spectrometry data (Fig S7) was acquired using a QSTAR quadrupole-TOF mass spectrometer with an electrospray ionization source. The unlabeled and labeled protein sample (2 mg/ml hVELC in 10 mM NH_4HCO3 buffer at pH 7.9) was injected into the solvent stream by using a 10 μl injection loop installed in the integrated loop injector. Three to five injections were performed for every sample, with 2-min intervals between them. Data were acquired continuously during load buffer infusion and protein infusions over the range 500–2,000 *m*/*z*. Spectra were analyzed with AnalystQS (Applied Biosystems) software.

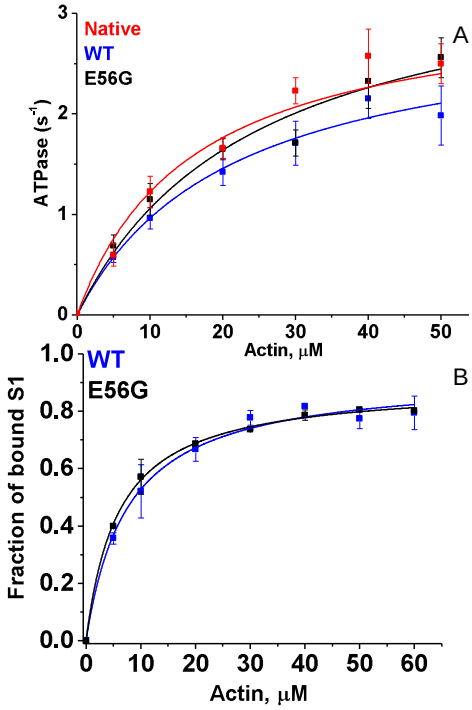

Fig. S3. (*A*) Actin-activated ATPase activity of cardiac myosin S1 constructs. (*B*) Binding of labeled myosin S1 constructs to labeled actin in the presence of saturating ATP, measured by co-sedimentation assays. V_{max}, K_{ATPase} and K_d values are summarized in Table 1.

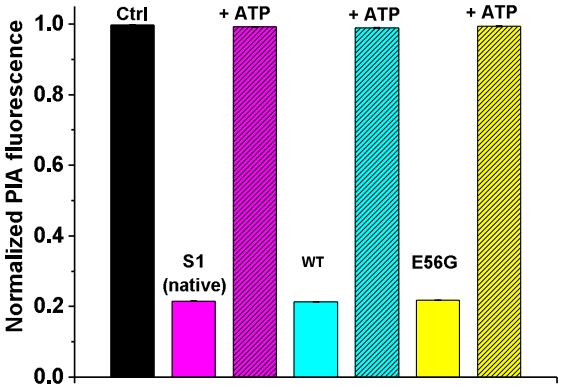

Fig. S4. Interaction of cardiac S1 with pyrene-actin (2 μM). Fluorescence was measured in F-Mg buffer at 25°C and normalized to the value obtained in the absence of S1 (Ctrl, black bar). Steady-state fluorescence in the presence of 10 μM S1 (of thee sources, as indicated) was measured in the absence (solid bars) and presence (shaded bars) of 3 mM (which was shown to be saturating) ATP. The results indicate that all three S1 samples quenched pyrene-actin to the same extent in the absence of ATP (within 1%), and no quenching (less than 1%) was observed in the presence of saturating ATP. Thus the E56G mutation has no detectable effect on the actin-myosin interface, as detected by pyrene-actin, in the absence or presence of saturating ATP.

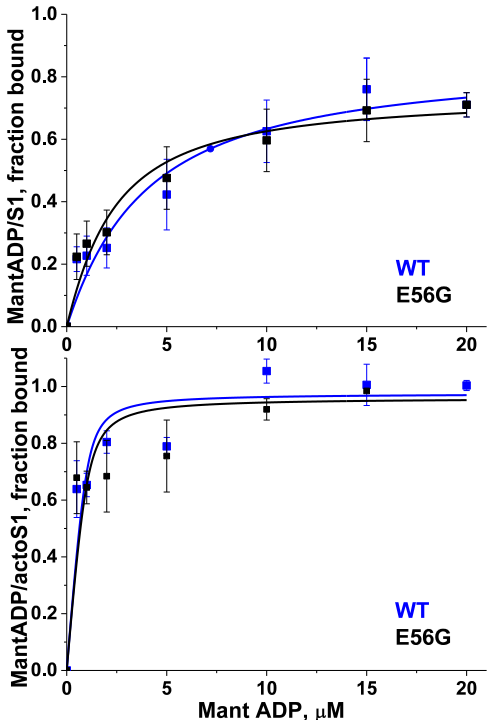

Fig. S5. Binding of cardiac myosin S1 constructs to MANT-ADP in the absence (top) and presence (bottom) of actin.

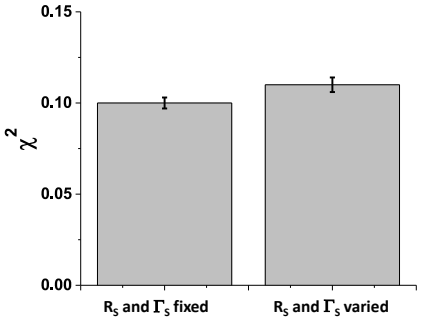

Fig. S6. χ^2 value for the fitting of the strong state (S) state parameters in the presence of ATP. No significant improvement in the fit (decrease in χ^2) was obtained by allowing the *S*-state parameters (R_S, Γ_S) to vary from the values observed in the absence of ATP.

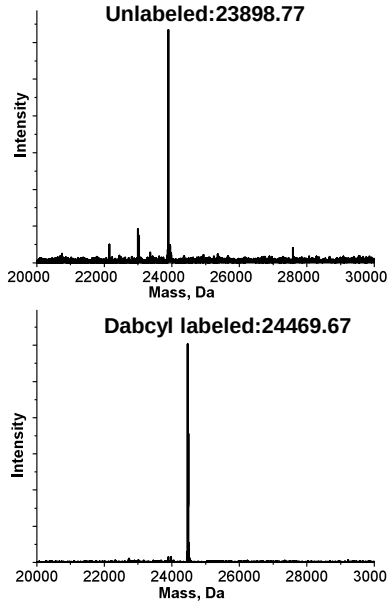

Fig. S7. ESI-MS spectra of unlabeled and Dabcyl labeled hVELC. Mass shift of 570.23 Da and absence of the unlabeled peak in the labeled sample shows complete labeling

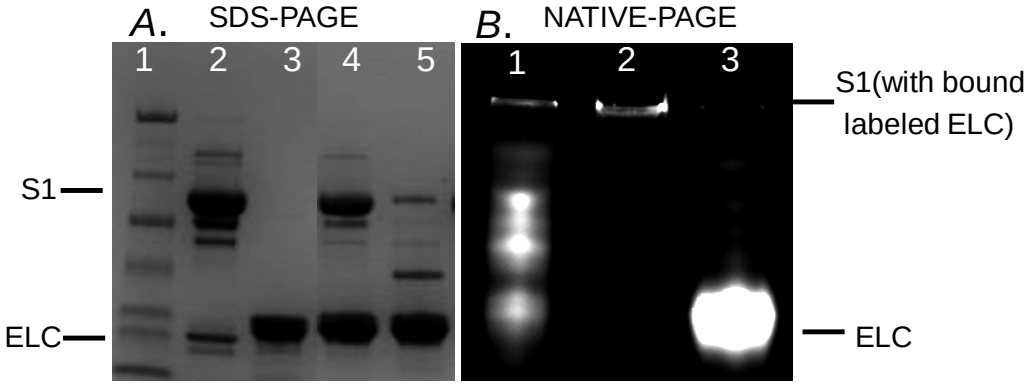

Fig. S8. SDS and Native PAGE of labeled and exchanged β-cardiac S1. A. SDS-PAGE. Lane 1: molecular weight marker, Lane 2: S1 before exchange, Lane 3: hVELC. Lane 4: Final S1 with exchanged ELC. Lane 5: Free ELC after spin down with actin. B. Native PAGE. Lane1: exchanged S1 before free hVELC separation. Lane 2: S1 used for experiment (no free hVELC). Lane 3: Free hVELC. Absence of free hVELC in lane 2 shows that the FRET signal is entirely from S1-bound ELC. Lane 4 in SDS-PAGE corresponds to Lane 2 in Native PAGE.

SUPPORTING REFERENCES

1. Kast, D., L. M. Espinoza-Fonseca, C. Yi, and D. D. Thomas. 2010. Phosphorylation-induced structural changes in smooth muscle myosin regulatory light chain. Proc Natl Acad Sci U S A 107:8207-8212.
2. Muretta, J. M., A. Kyrychenko, A. S. Ladokhin, D. Kast, G. E. Gillispie, and D. D. Thomas. 2010. High - performance time-resolved fluorescence by direct waveform recording. Rev Sci Instrum 81:103101-103101 - 103101-103108.
3. Lakowicz, J. R. 1999. Principles of Fluorescence Spectroscopy. New York: Kluwer Academic/Plenum Press.
4. Guhathakurta, P., E. Prochniewicz, and D. D. Thomas. 2015. Amplitude of the actomyosin power stroke depends strongly on the isoform of the myosin essential light chain. Proc Natl Acad Sci U S A 112:4660-4665.
5. Agafonov, R. V., I. V. Negrashov, Y. V. Tkachev, S. E. Blakely, M. A. Titus, D. D. Thomas, and Y. E. Nesmelov. 2009. Structural dynamics of the myosin relay helix by time-resolved EPR and FRET. Proc Natl Acad Sci U S A 106:21625-21630.